Chloride induced mechanical degradation of ultra-high performance fiber-reinforced concrete

Document Version:
Publisher's PDF, also known as Version of Record (includes final page, issue and volume numbers)

Please check the document version of this publication:

• A submitted manuscript is the version of the article upon submission and before peer-review. There can be important differences between the submitted version and the official published version of record. People interested in the research are advised to contact the author for the final version of the publication, or visit the DOI to the publisher's website.
• The final author version and the galley proof are versions of the publication after peer review.
• The final published version features the final layout of the paper including the volume, issue and page numbers.

Link to publication

Chloride induced mechanical degradation of ultra-high performance fiber-reinforced concrete: Insights from corrosion evolution paths

Zhaoping Song [a], Shaohua Li [a], Qingliang Yu [a,b,*]

[a] School of Civil Engineering, Wuhan University, 430072 Wuhan, PR China
[b] Department of the Built Environment, Eindhoven University of Technology, P.O. Box 513, 5600 MB Eindhoven, The Netherlands

ARTICLE INFO

ABSTRACT

Chloride-induced corrosion of ultra-high-performance fiber-reinforced concrete (UHPFRC) inevitably affects structural durability. However, the process of multi-fiber corrosion and mechanical deterioration still lacks sufficient understanding. This work aims to reveal the fiber corrosion degradation mechanism from a microscopic to macroscopic view, applying multiple analytical analyses of atomic absorption spectrometry, SEM-EDS, nano-indentation, polarization, and macroscopic mechanical testing. Results show that the flexural strength of specimens decreases significantly with the increase of corrosion degree, and a clear reduction of up to 47% is found at a high corrosion degree. Elastic modulus and nano-hardness of corroded samples vary in a wide range of 30–189 GPa and 0.16–6.41 GPa. With the increase in fiber content, two distinctive corrosion mechanisms are proposed. The corrosion path deteriorates from fiber edge to inner by the invasion of erosive solution through the matrix at low contents (<2 vol%). Considering impurities, greater interfacial defects and macro-cell potential differences at high contents (≥2 vol%), another corrosion path originates from the fiber inner outward to the matrix. Fiber corrosion damages the fiber's structural integrity and induces matrix deterioration, the micromechanics of the matrix along the fiber edge 20 μm decreases at least 10% more than the concrete matrix. This work firstly sheds light on the mechanical deterioration of UHPFRC from the perspective of fiber corrosion paths considering different initiation scenarios.

1. Introduction

Steel fiber distributed in Ultra-high performance fiber-reinforced concrete (UHPFRC) can play an effective bridging role, by alleviating stress concentration and restraining crack propagation of structure, and increasing energy absorption before failure [1–5]. Previous studies claim that UHPFRC with a high-quality dense structure has a much lower corrosion risk compared to plain concrete [1,6–10]. However, a complex environment with a large number of erosive ions poses a great threat to steel fibers in Ultra-high performance concrete (UHPC) due to its iron nature, which increases the corrosion possibility of UHPFRC [11,12]. Inevitably, microstructure defects of micro-cracks generated during the process of manufacturing and engineering services, as well as the poor interface between fibers and the surrounding matrix, are responsible for the occurrence of steel fiber corrosion [12–15]. Once the corrosive solution reaches the surface of the steel fiber through microcracks, it will cause corrosion of the steel fiber, and the interactive steel fiber itself will accelerate the macro-cell corrosion development of UHPFRC.

Fiber corrosion would strongly impair the structure durability [11,16–19]. Previous studies related to detrimental effect of fiber corrosion on UHPFRC mainly focus on macro-mechanical performance [11,20–23]. Most researchers agree that multi-fibers corroded in UHPFRC could reduce mechanical strength, resulting from corrosion of bridging fibers, corrosion cracking and cambia spalling of concrete [11,20,24,25]. For strength degradation caused by fiber corrosion, some conceptual mechanisms have been proposed. Song et al. [11] and Fan et al. [24] attributed strength reduction of fiber-reinforced concrete to increase of connecting conductive fiber amounts in which formation of conductive pathways accelerates occurrence of corrosion. Lv et al. [15,20,26] reported that the lower mechanical performance is derived from continuous invasion of chloride ions, which would cause fiber corrosion and induce corrosion cracking with the expansion force produced by corrosion products in severe cases. Meson et al. [19,25] argued that corroded steel fiber, deterioration of matrix around crack and steel fiber–matrix interface have adverse effects on long-term mechanical

---

properties of structure. Previous researches have assigned the essential reason for degradation of macroscopic mechanical properties to transformation in internal microstructure. But variation of microstructure in fibers corrosion affecting deterioration of mechanical properties in UHPFRC is still unclear, especially how corrosion evolution paths of steel fiber differ significantly at different fiber contents and corrosion degree.

As mentioned above, investigation of micro level on fiber corrosion in UHPFRC is scarce. In previous study [20], although the influence of steel fiber corrosion on tensile mechanical properties of UHPFRC is researched from micro level, only morphology of microstructure is evaluated. They do not involve quantitative characterization of micro mechanics caused by microstructure change and fiber contents induced variation of corrosion evolution process. So, mechanical degradation in UHPFRC is not fully characterized from microscopic perspective. In reality, stress area of steel fiber is damaged when concrete structure is subjected to corrosive environment [27,28]. Besides, with aggravation of corrosion, hardness of matrix decreases sharply, resulting in the decrease of bonding property between fiber and local matrix [29,30]. Consequently, internal microstructure will be changed, resulting in gradual deterioration of interface between steel fiber and matrix by increased fiber corrosion, and degraded matrix by the expansion force of corrosion products. It is inevitable that above changes will lead to the transformation in micromechanics, which will affect cracking strength of concrete structure. Moreover, it is not clear whether corroded steel fiber can still effectively bridge matrix and continue to exhibit good strain hardening properties in UHPFRC. Therefore, steel fiber corrosion of UHPFRC from the perspective of microstructure and micromechanics should be studied, and its influence on macroscopic mechanical properties requires to be surveyed, which has never been reported thus far.

In most of the investigations on steel fiber corrosion, electrochemical accelerated corrosion is employed [15,20,24,26], especially considering the dense structure of UHPC where natural corrosion is too time consuming [21,31]. Chen et al. [15,26] investigated the corrosion behavior and mechanical performance of reinforced SFRC using impressed direct current until target corrosion degrees were reached. Nevertheless, most studies applying accelerated corrosion are based on only a single steel bar or one steel fiber to investigate reinforcement corrosion development in UHPC [24,32,33], which goes against original intention of multi-fiber corrosion characterization of UHPFRC. Since resistance of matrix is much higher than that of steel fiber, multi-fibers in UHPFRC are not as easily corroded as only one rebar by direct current. In order to explore the influence of fiber corrosion on macroscopic mechanical properties in UHPFRC, corroded steel fibers are often directly added to fresh UHPC paste that even shows an improvement in mechanical properties [34]. The result is controversial which ignores that fiber corrosion is a dynamic evolution process and will have an impact on surrounding matrix. Hence, it is imperative to propose a new reliable accelerated corrosion method for UHPFRC.

This work aims to shed light on corrosion evolution and deterioration of mechanical performance in UHPFRC from perspective of micromechanics. Electro-chemical workstation, as a bridge between microscopic change and macroscopic degradation, is applied to characterize electro-chemical characteristics of different fiber corrosion degrees in UHPFRC. The concentration of Fe^{3+} in leachate is measured by atomic absorption spectrometry (AAS) to quantitatively characterize corrosion degree of UHPFRC at different positions. Then, scanning electron microscope (SEM) is applied to characterize micro-structure of fiber corrosion, and the propagation of steel-fiber corrosion-induced defects such cracks and pores. In addition, the distributions of erosive elements and dissolved iron are analyzed by energy dispersive spectrometry (EDS). Moreover, nano-indentation is used to quantify micromechanical properties in corroded/non-corroded area of fiber and matrix. Lastly, strength test including compressive strength and three-point flexural measurements is used to study the influence of fiber corrosion on mechanical properties, and the strain hardening relationship

between fiber content and corrosion degree. Through these multi-scale observations, corrosion evolution paths of fiber induced mechanical degradation in UHPFRC are systematically studied, accounting for the relationship between fiber contents and corrosion degree.

2. Experimental approach

2.1. Materials and specimen preparation

The designed mixture presented in Table 1 were employed to prepare samples. Class Cement PII● 52.5, micro-silica and limestone were used as binders to prepare UHPC with a constant water to binder ratio of 0.18. Chemical and physical properties of used powder were analyzed by X-Ray Fluorescence (XRF), gas pycnometer (AccuPyc 1340 II Pycnometer) and Brunauer Emmett Teller (BET), respectively, as shown in Table 2. Microstructure of used powders was presented in Fig. 1 (a ~ c), which is measured by SEM. In addition, quartz sand with four kinds of particle size fractions (124–250 μm, 250–420 μm, 420–840 μm, 840–2000 μm) were used as aggregates. The particle size distribution of above-mentioned materials was analyzed by sieve and laser particle size analyzer (Bettersize 2000E), presented in Fig. 1(d). The straight steel fiber with a length of 13 mm and diameter of 0.2 mm was applied with 5 different volume amounts of 1%, 1.5%, 2%, 2.5% and 3%, respectively. Table 3 showed the geometrical and physical properties of used fibers. The liquid polycarboxylate-based superplasticizer with a solid content of 30% was incorporated in the mixture to acquire self-consolidating property as well as to help to disperse steel fibers.

The fresh UHPFRC were cast into the mold of $40 \times 40 \times 160$ mm^3, detailed preparation process was shown in Fig. 1 (e). Then all fresh UHPFRC prism were sealed with plastic wrap and stored in the curing chamber at 20 ℃ for 24 h. Subsequently, all specimens were demolded and cured in water in the curing chamber at 20 ℃ until 28 days. Accelerated corrosion tests were carried out with different duration after 28 days curing period, which can obtain a unified initial condition to investigate the degradation mechanism of corroded UHPFRC with different degree.

2.2. Test methods

2.2.1. Accelerated corrosion

Before accelerated corrosion or electrochemical test, all specimens were saturated in vacuum. In order to simulate a stable corrosion environment, a constant voltage at 60 V was applied to all specimens by DC galvanostatic. Corrosion cycles were 0, 14 and 28 days with the aim to fabricate three corrosion degrees of I, II and III. Details of accelerated corrosion test were shown in Fig. 2, CFRP cloth was used to cover specimen's surface. In order to prevent water evaporation, outer layer of CFRP cloth was wrapped with waterproof materials (positive electrode), and 40×60 mm^2 stainless steel plate served as the negative electrode. Then the prepared specimen and stainless steel were placed in the 3.5 % salt solution together. It should be noted the naming principle of

Table 1
Mixture proportion.

Quantities	Mass (kg/m^3)
P·II 52.5 cement	712.5
Micro-silica	47.5
Limestone powder	190
Superplasticizer	19
Water	158
Sand 1# (840–2000 μm)	483.2
Sand 2# (420–840 μm)	338.2
Sand 3# (250–420 μm)	132.9
Sand 4# (124–250 μm)	253.7
Steel fibers	1%, 1.5%, 2%,2.5%, 3% by total volume of mixture
Water-binder ratio	0.18

Table 2
Chemical and physical properties of powders.

Substance (%)	CaO	SiO$_2$	Al$_2$O$_3$	Fe$_2$O$_3$	SO$_3$	MgO	TiO$_2$	Mn$_3$O$_4$	LOI	Specific density(g/cm^3)/BET surface area(m^2/kg)
cement	64.61	19.20	4.17	3.69	3.33	1.31	0.22	0.10	2.04	2.99/944
micro-silica	0.05	96.33	0.16	0.28	/	/	/	/	0.88	2.23/9716
limestone	53.55	0.62	/	0.01	1.88	0.64	/	0.01	42.63	2.75/1353

designed specimen, e.g. U1-I/II/III. Number 1 to 3 and I / II / III represent UHPFRC sample with fiber amounts from 1 vol% to 3 vol%, corrosion degree of no corrosion (I), slight corrosion (II) and heavy corrosion (III), respectively.

2.2.2. The determination for chloride diffusion depth

The penetration depth of chloride ions was measured by AgNO$_3$ [29]. The AgNO$_3$ solution was sprayed on the split surface of 40 × 40 mm^2 chiseled from the middle of designed specimen. AgCl (white precipitation) generated on the surface can be used to determinate the diffusion depth of chloride ion, presented in Fig. 3.

2.2.3. Iron concentration measurements

In addition, atomic absorption spectrometry (contrAA700) was employed to quantitatively determine iron ion concentration in corrosion area of sample at the location of 0–4 mm, 8–12 mm and 16–20 mm, respectively, considering that corrosion is triggered from external surface. Each split prism was separated by three areas to collect representative data. Samples were chiseled from same longitudinal split section, on a three contour profiles with 4 × 40 mm^2 area and 1.0 mm ± 0.1 mm: at an equal spacing of 4 mm in Y-axis, presented in Fig. 3. After removing steel fibers, three blocks chiseled from same depth were ground into powder. Powdered samples at selected area were collected, each totaling at least 2.0 g to complete iron concentration measurements. Then the powder was pretreated by acid and diluted with deionized water. High-speed centrifuge was used for solid–liquid separation after oscillation by a vibrating machine for 24 h, and finally settled solution was extracted for testing. Iron ion concentration was expressed by mg/L.

2.2.4. SEM and EDS analyses for steel fiber corrosion evolution

In this section, areas including evolution zones among non-corroded steel fiber, corroded steel fiber, steel fiber edge and matrix were selected for microstructural analysis by scanning electron microscope (TESCAN MIRA3). Processing steps of samples for SEM-EDS analysis were as follows: first, a UHPFRC block with a size of 15 mm × 20 mm × 5 mm was cut from fracture prism, immersed in alcohol to terminate hydration and dried in the oven. Then, each block was placed into the cylinder mold with a diameter of 25 mm and a height of 20 mm and filled with epoxy resin. Finally, samples were further treated by polishing with 400, 800 and 1200 mesh sandpapers to smooth surfaces and finally coated with gold for both secondary electron images (SE) and backscattered electron images (BSE) observations. A Gemini 500 SEM analyzer equipped with an energy dispersive spectrometer (EDS) was applied to observe microstructure of fiber corrosion in UHPFRC, with an accelerating voltage of 30 kV. This analyzer had a high resolution which can investigate fiber surface morphology and micro cracks, respectively. EDS spectra were applied to determine the distribution of elements in corrosion area of steel fiber, mainly including copper, iron, oxygen, chloride, and silicon. The distribution and content of oxygen can be identified as the regional distribution of corroded steel fibers.

2.2.5. Nano-mechanics degradation caused by fiber corrosion

The sample was processed into cylinder with a diameter of 25 mm and a thickness of 20 mm to measure nano-mechanics evolution caused by fiber corrosion. In order to acquire a representative data [35], it was necessary to use diamond polishing machine to do a coarse grinding and polishing for sample. Processing process of coarse grinding and polishing were described as following. Samples are ground by 400, 800, and

1200 grit abrasive paper with each step last for 15 min, and polished by 9, 3, 1 μm polishing cloth with oil-based diamond suspension for at least 30 min/step. Alcohol was continuously used to contact the sample surface during the grinding and polishing process. Then, samples were washed in ultrasonic cleaner with alcohol. Finally, samples were placed in a vacuum drying oven at 40 ℃ for 24 h, sealed and stored in the desiccator until testing.

Ti950 triboindenter nano-indentation apparatus manufactured by Hysitron Company was used to obtain the relevant nanoscale mechanics parameters in this work. 10 × 10 grids with a grid spacing of 20 μm are applied for each measured area, and 100 indentation points were collected. The data processing process of nano-indentation was shown in Fig. 4. The fiber edge was taken as the reference line for analysis, and the spacing cycle of elastic modulus/hardness distribution in the sample was 20 μm. The selected scanning points of non-corroded/corroded steel fiber, fiber edge and matrix fall on the circumference with diameters of 0 to 60 μm, 80 to 100 μm and 120 to 180 μm, respectively, as detailed in Fig. 4. The indentation hardness (H), indentation modulus (M) and the elastic modulus of the testing point (E) were calculated applying eqs. (1–3) according to the classic Oliver-Pharr principle [36].

$$H = \frac{P_{max}}{A_c} \tag{1}$$

$$M = \frac{\sqrt{\pi}}{2\beta} \frac{S}{\sqrt{A_c}} \tag{2}$$

$$E = (1 - v^2)\left[\frac{1}{M} - \frac{(1 - v_i^2)}{E_i}\right]^{-1} \tag{3}$$

where, P_{max}, A_c and S represent peak load, contact area at the point of peak load and the slope at the top of the unloading curve, respectively. β and v are the constant indenter correction coefficient depending on Berkovich indenter geometry, and poison's ratio in cement-based materials, respectively. v_i and E_i are the poison's ratio and elastic modulus of indenter, respectively. A diamond indenter is employed in this paper, with $\beta = 1.034$, v $= 0.25$, $v_i = 0.07$, $E_i = 1141$GPa [37].

2.2.6. Bridging role by Tafel polarization test

Accelerated corrosion was an electrochemical process that can accurately assess the corrosion potential and current density of fiber-reinforced cement-based materials by Tafel polarization curve [24,38]. Polarization testing can help to reveal the relationship between microstructure evolution and macroscopic mechanical degradation of fiber corrosion in UHPFRC. A standard 40 × 40 × 160 mm^3 specimen was placed in electrolyte and measured by three electrodes. The working electrode was connected to copper, the opposite electrode to stainless steel, and the auxiliary electrode to Hg electrode. An open circuit potential test was performed for at least 60 min to obtain a stable voltage before Tafel polarization testing.

2.2.7. Degradation characterization of macroscopic mechanical properties

Afte electrochemical test, three-point flexural test was applied to evaluate flexural properties (e.g. ultimate load, mid-span deflection, cracking in real-time) of UHPFRC at a loading rate of 0.2 mm/min [9], using a commercial mechanical testing machine with a maximum loading capacity of 100 kN. The designed span length was 100 mm, and the beams were revolved 90° from casting coarse surface to reduce
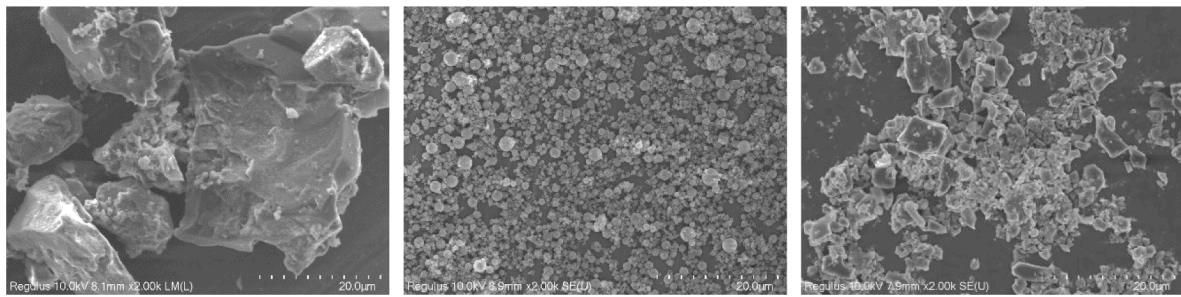
(a) Cement 52.5   (b) Micro-silica   (c) Limestone powder
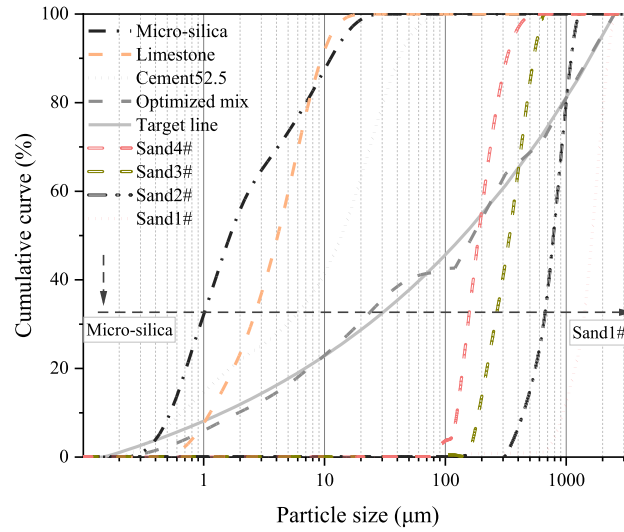
(d) Particle size distribution
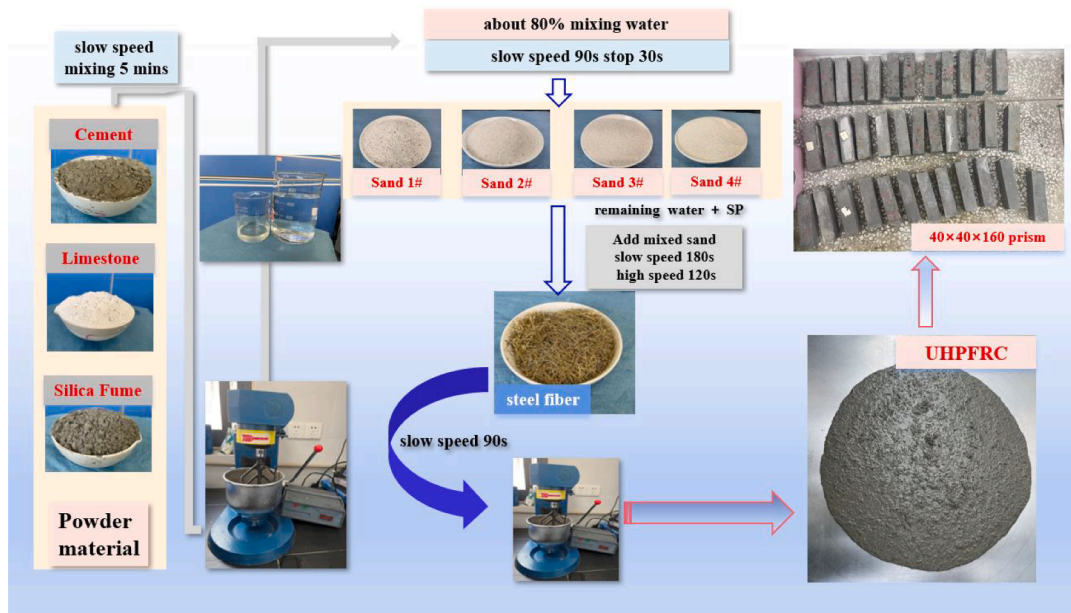
(e) Sample preparation process

Fig. 1. Illustration of raw materials: (a ~ c) SEM images of powders, (d) Particle size distribution, (e) Sample preparation process.

Table 3
Property of steel fiber.

Diameter (mm)	Length (mm)	Aspect ratio	Density (g/cm^3)	Tensile strength (MPa)	Elastic modulus (GPa)
0.2	13	65	7.9	2500	200

decentered effect, shown in Fig. S5 (Supplemental Information). After flexural test, compressive strength experiment was carried out to split specimens.

3. Experimental results

### 3.1. Surface morphology and water-soluble chloride distribution caused by corrosion

The images of UHPFRC specimen in Fig. 5 showed an obvious corrosion damage. Clearly, corrosion area or concrete spalling became more and more serious with the increase of steel fiber contents and corrosion degree. It is attributed to that the more fiber content is, the smaller spacing is (see Fig. 5 (a)), which can easily form an effective lapping in matrix and accelerate the development of corrosion [11,20]. It can be observed that the corrosion area expanded that caused a looser structure or even spalling of concrete cover, as presented in Fig. 5 (b,c).

When there was no corrosion damage, the penetration depth of chloride ions was almost negligible. No matter how many steel fibers are present, it is difficult for chloride ions to invade UHPC due to the dense structure [39]. The measured chloride depth of UHPFRC with various fiber amounts at corrosion degree II and III were presented in Fig. 6 (a). Chloride ion penetration depth of UHPFRC incorporating 1 vol%, 1.5 vol%, 2 vol%, 2.5 vol% and 3 vol% at corrosion degree of II were 4.34, 4.35, 7.05, 7.44 and 8.43 mm, respectively. Meanwhile, chloride ion penetration depth in corroded UHPFRC with the same fiber amounts at corrosion degree of III was gradually increased to 9.7, 11.79, 12.47, 16.74 and 18.48 mm, respectively. As can be noticed, chloride ion penetration depth of corrosion II and III were gradually increased from 1% to 94% and 22% to 91%, respectively, with the increase of fiber amounts from 1.5 vol% to 3 vol%, compared with that of 1 vol%. Chloride ion penetration depth of U-III samples with five fiber contents were found 2.24, 2.71, 1.77, 2.25 and 2.19 times greater than that of corrosion II ones, respectively. Therefore, all chloride ion penetration depth were enlarged with the increase of fiber contents and corrosion degree. The results above can be explained that fiber corrosion in UHPFRC occurs when the chloride ion content exceeds the threshold, which is related to matrix porosity and exposure condition [40,41], as well as fiber contents [11]. The larger diffusion of the UHPFRC with higher fiber contents is mainly due to the weak interfacial area between fibers and paste, resulting in a higher interfacial porosity [42,43]. The steel fibers with a smooth surface serve as a wall to prevent the uniform distribution of hydration products, generating a discontinuous region. The wall effect of steel fibers prevents the precipitation and uniform distribution of hydration products [42,44]. Also, more air pores would be formed around the fibers, resulting from the discontinuous structure of hydration products. Therefore, steel fibers induce the increase of interfacial porosity to a certain extent, and at the same time, they are easy to generate a network in the UHPFRC matrix, which provides a circuit path for fiber corrosion during the erosion process [11,45]. The present results indicated that when steel fiber content exceeds 2 vol%, abundant fibers can effectively connect to each other, which increases the diffusion of chloride ions and causes the dissolution of iron, resulting in the increase of corrosion degree. In addition, with a longer erosion time, chloride ions continue to invade, which deepen the fiber corrosion and deteriorate concrete, shown as cracking and spalling, leading to a more serious corrosion degree.

3.2. Fiber corrosion evolution determined by iron concentration

To determine corrosion degree, atomic absorption spectrometry analysis was performed. Fig. 6 (b) displayed the iron concentration (Fe^{3+}) at three specific distances of 0–4, 8–12 and 16–20 mm from sample surface. Iron concentration of each specimen decreased from outside to inside, and it is clear that the corrosion of UHPFRC first occurred in outer layer. There was no obvious local variation in U2-I, in which the measured values of position 1, 2 and 3 varied between 67.8 and 74.1 mg/L. As expected, the concentration of Fe^{3+} at specific position height increased with the increase of fiber contents and corrosion degree, indicating the deepening of corrosion. For instance, the values of U-III at the surface were steadily increased from 327.1 to 343.9 mg/L and reached the highest value of 597.2 mg/L, with the increase of fiber contents from 1 vol% to 3 vol%. Compared with U2-I, Fe^{3+} concentration of U2-II at 0–4, 8–12 and 16–20 mm were increased by 2.31, 0.46 and 0.28 times, while U2-III at the addressed location were increased by 4.07, 1.80 and 1.12 times, respectively. Results may be explained as follows: chloride ion has a great impact on the corrosion resistance of steel fiber, causing dissolution of fibers. The more fiber contents, the larger porosities are introduced, and the stronger conductive network are [11,45]. Moreover, with the increase of exposure time, specimen has accumulated enough chloride ions to destroy the passivation layer of fiber. The iron becomes ionized state and continuously dissolves in matrix, resulting in the increase of Fe^{3+} concentration and causing pitting corrosion or even heavy corrosion of fibers.
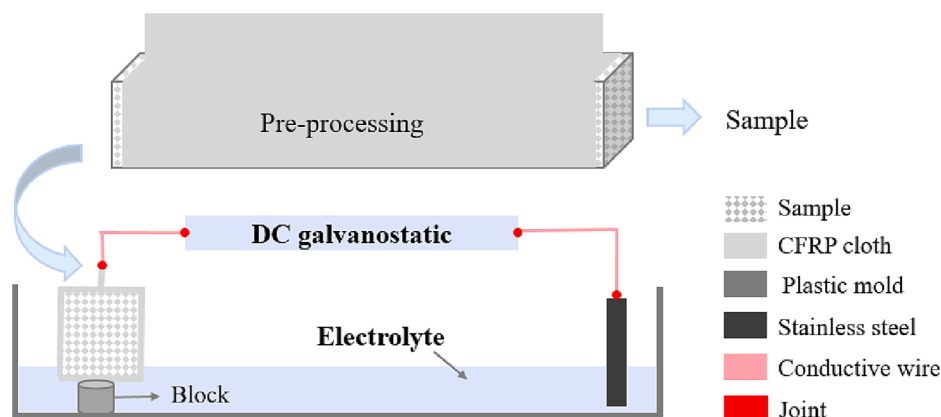
Fig. 2. Schematic diagram of pre-processing and accelerated corrosion of UHPFRC.
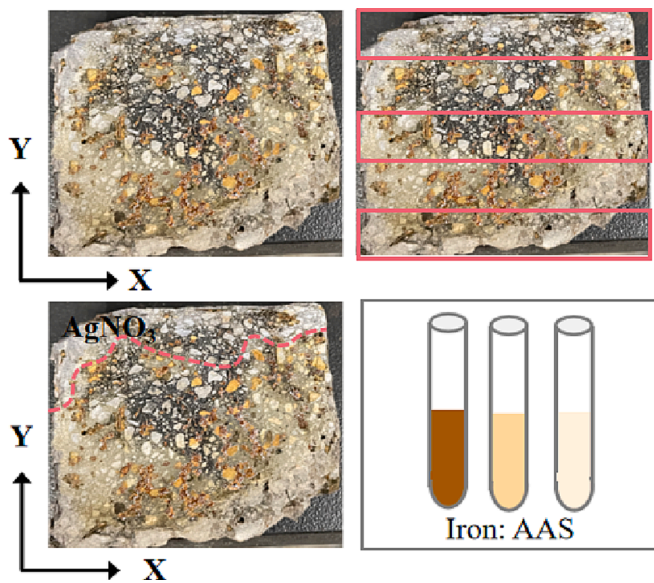
Fig. 3. The diagram of colorimetric indicators AgNO$_3$ for chloride depth detection (left) and the selected location for iron concentration testing (right).
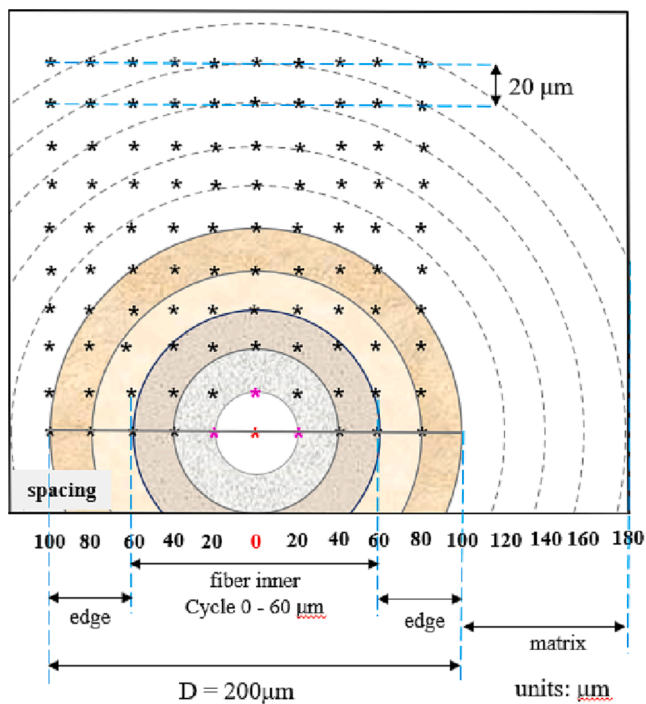

Fig. 4. Schematic diagram for nano-mechanism distribution of the designed UHPFRC.

3.3. Corrosion induced degradation in microstructure and micromechanics

To further understand the degradation of micromechanics and microstructure induced by fiber corrosion, specimens for micro-mechanical and microstructural testing were extracted from the prism samples subjected to various corrosion degree of I, II, III.

3.3.1. Microstructure analysis applying SEM-EDS

Fig. 7 (a) and S1 (Supporting information) presented the SEM image of the cross section of designed sample, accompanied by EDS analysis. For each specimen, several areas of interest were scanned to obtain a similar overall image, where the analysis area of fiber center, fiber inner, fiber edge and matrix were marked as spot 1, 2, 3 and 4 in Fig. 7 (b) and S1, respectively.

In this section, ten samples were used to characterize the micro-structure for all test specimens with five fiber contents at two corrosion degree (II, III), except the case of no corrosion damage, from which only the sample with 2.5 vol% (U2.5-I) was selected. It can be observed that there were no obvious dissolution of iron and rust in the case of Corrosion I, and the matrix around fiber was compact, presented in Fig. S1. When corrosion developed, sample U2.5-II showed some obvious cracks and pores, which accelerated the penetration of chloride ions and oxygen (see in Fig. S1). By corrosion degree III, steel fiber gradually dissolved and split heavily by corrosive substances, and corrosion products continuously permeated into matrix, shown in Fig. 7. Thus, with the same steel fiber content, steel fiber was continuously corroded and dissolved with the increase of corrosion degree. In addition, the dissolution and corrosion of fiber increased with the increasing fiber contents under the same corrosion degree, which was verified by U1, U1.5, U2, U2.5 and U3 of corrosion degree II/III in Figs. 7 and S1.

New defects such as cracks and pores are formed and connected due to the steel fiber corrosion. Once subjected to corrosion, fiber corrosion deepens through the existing micro-defects which provide open channels to erosion. Further, newborn defects are generated by the expanding force of corrosion products. The new micro-cracks are generated in the matrix especially near fibers due to the expanding force of fiber corrosion, resulting in a greater deterioration with the increased corrosion time or fiber contents under the same comparable condition. These serious corrosion phenomena can be ascribed to the following reasons: 1) adding fibers to UHPC leads to a weak interface in matrix around steel fibers [14,46], which facilitates the invasion of corrosive substances; 2) a number of conductive fibers effectively lapping in matrix would generate an abundant circuit pathway. Fiber corrosion is aggravated by the action of ion current from corrosive substances and internal spontaneous current; 3) interstitial impurities (such as S, Mn, Cu, Zn, Ti, etc., confirmed by EDS analysis and partly provided in Fig. S2) are generated during fiber production. Crevice corrosion and pitting corrosion of fiber occur in the existence of interstitial impurities, which is similar to the crevice corrosion mechanism of crack between rebar and mill scale [47]. Under the action of electrical current and ion current, fibers have different degrees of splitting (such as U1-II, U2.5-III) due to the non-uniform impurity interface of fiber itself. Furthermore, steel fibers split seriously, e.g. U1.5/2-II and U1/2/2.5-III, presented in Figs. 7 and S1. The loss of steel fiber hardness strongly deteriorates the macroscopic mechanical properties of UHPFRC.

The quantitative EDS analysis of Figs. 7 and S1 were summarized in Table 4, revealing all designed samples to investigate corrosion evolution. Measured values of Cl concentration and Fe/O atomic ratio varied significantly with different fiber contents and corrosion degree. There were two trends of chloride concentration among fiber center/edge and matrix. The first was that the concentration of chloride ions in matrix was higher than fiber edge, and fiber center is the lowest, as observed in Table 4 of U1/U2/U2.5-II and U1/U2.5/U3-III which can be explained that chloride ions continuously erode steel fiber through matrix. Due to the dense structure of UHPFRC matrix, chloride ions continuously erode the matrix first, leading to a high concentration of chloride ions in matrix. The second trend of chloride concentration was: steel fiber center > steel fiber edge > matrix, e.g. U1.5/U3-II and U2-III. It can be mainly attributed to that erosive solution continuously accumulates in fiber inner along the weak interface provided by impurities, leading to the rapid deterioration of inner fiber where obvious holes are present than outer fiber.

In addition, the decreasing Fe/O atomic ratio was affected directly by the increasing corrosion degree. For instance, at a given fiber volume amount of 2.5%, the Fe/O atomic ratio of U2.5-I, U2.5-II and U2.5-III at the selected position of matrix were 2.8, 1.82 and 0.06, while 2.35, 0.55 and 0.34 in fiber edge, respectively, which means that the most severe
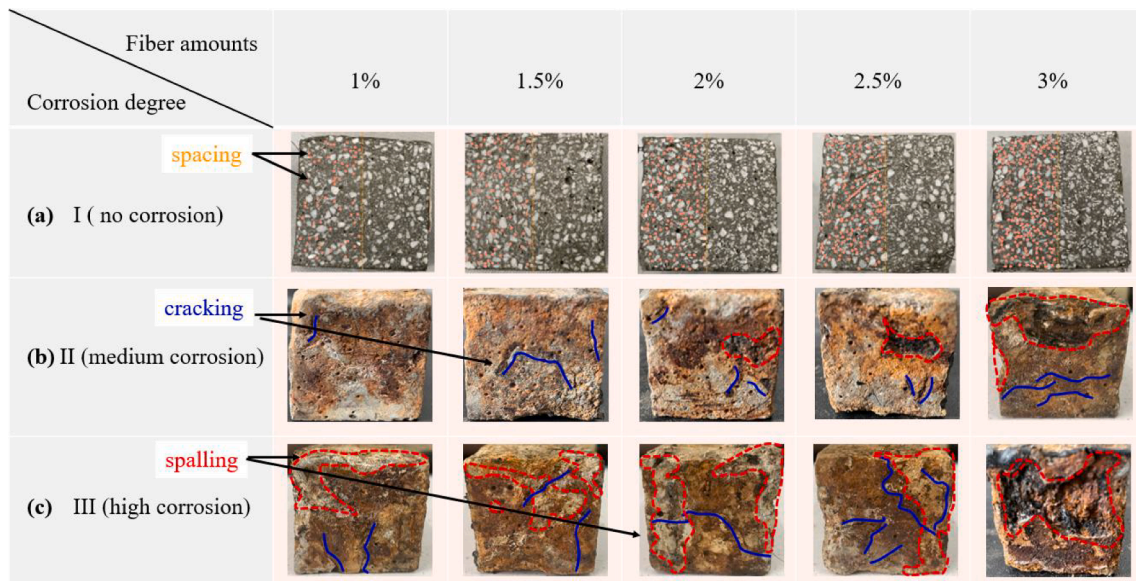
Note: corrosion-induced cracking (blue), concrete surface spalling caused by corrosion (red)

Fig. 5. Surface morphology on UHPFRC with three corrosion degree and five fiber amounts. **Note: corrosion-induced cracking (blue), concrete surface spalling caused by corrosion (red)**. (For interpretation of the references to colour in this figure legend, the reader is referred to the web version of this article.)

(a) Chloride ion penetration depth

(b) Iron concentration
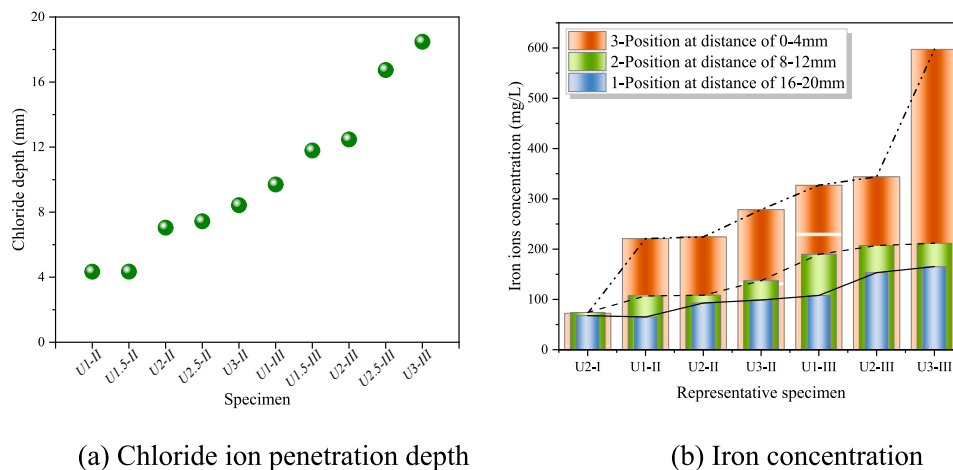
Fig. 6. Measured values in the designed UHPFRC specimen.

damage was obtained in the case of corrosion III and steel fiber corrosion gradually spreaded inwards. Nevertheless, there was still a slight local change in each Fe/O atomic ratio of sample with various fiber amounts under the same corrosion degree. For example, the Fe/O atomic ratio in fiber edge was 0.49, 0.65, 0.31, 0.50 and 0.32 from 1 vol% to 3 vol% of corrosion III, respectively. It can be seen roughly that Fe/O atomic ratio of steel fiber decreased with the increase of fiber contents, and the dissolution and corrosion of steel fiber occurred more easily with higher fiber contents. This can be explained by following reasons: 1) fiber contents directly affect the overlapping network and circuit. Better lapping network, faster corrosion process is. 2) iron dissolves gradually and corrosion products are generated with the constant invasion of chloride and oxygen, leading to a complex composition of corrosion products. Then different phases of corrosion products can be mixed to different degrees. As a result, their crystallization state differed from each point [48,49], showing a Fe/O atomic ratio of 0.49 in sample with 1 vol% higher than that of 0.31 in sample with 2 vol%.

3.3.2. Nano-mechanical results

To quantitatively identify the evolution of micro-mechanical properties from undamaged/damaged fiber inner - fiber edge to matrix, average elastic modulus was plotted against the distance from center line of region in steel fiber (presented in Fig. 4). Fig. 8 (a-c) represented the contour maps of elastic modulus for U2.5-I/II/III groups, the remaining groups were shown in Fig. S3. Non-corroded steel fiber possessed the highest elastic modulus values (greater than 200 GPa) in this work, which was in good accordance with steel rebar without corrosion [50,51]. It is reported that elastic modulus of corroded reinforcement would show a decreasing trend [48,52].

As summarized in Fig. S3, the elastic modulus and hardness of steel fiber and matrix decreased sharply with corrosion of fibers. As expected, the elastic modulus increased with nano-hardness. The elastic modulus of steel fiber gradually decreased, ranging from 186 GPa to 26 GPa, and the nano-hardness decreased from 7.40 to 0.30 GPa, with the increasing degree of corrosion. The elastic modulus of fiber edge was slightly lower than that of fiber inner, indicating that corrosion of steel fiber originated from fiber edge. Although fiber edge was corroded, it still had a higher
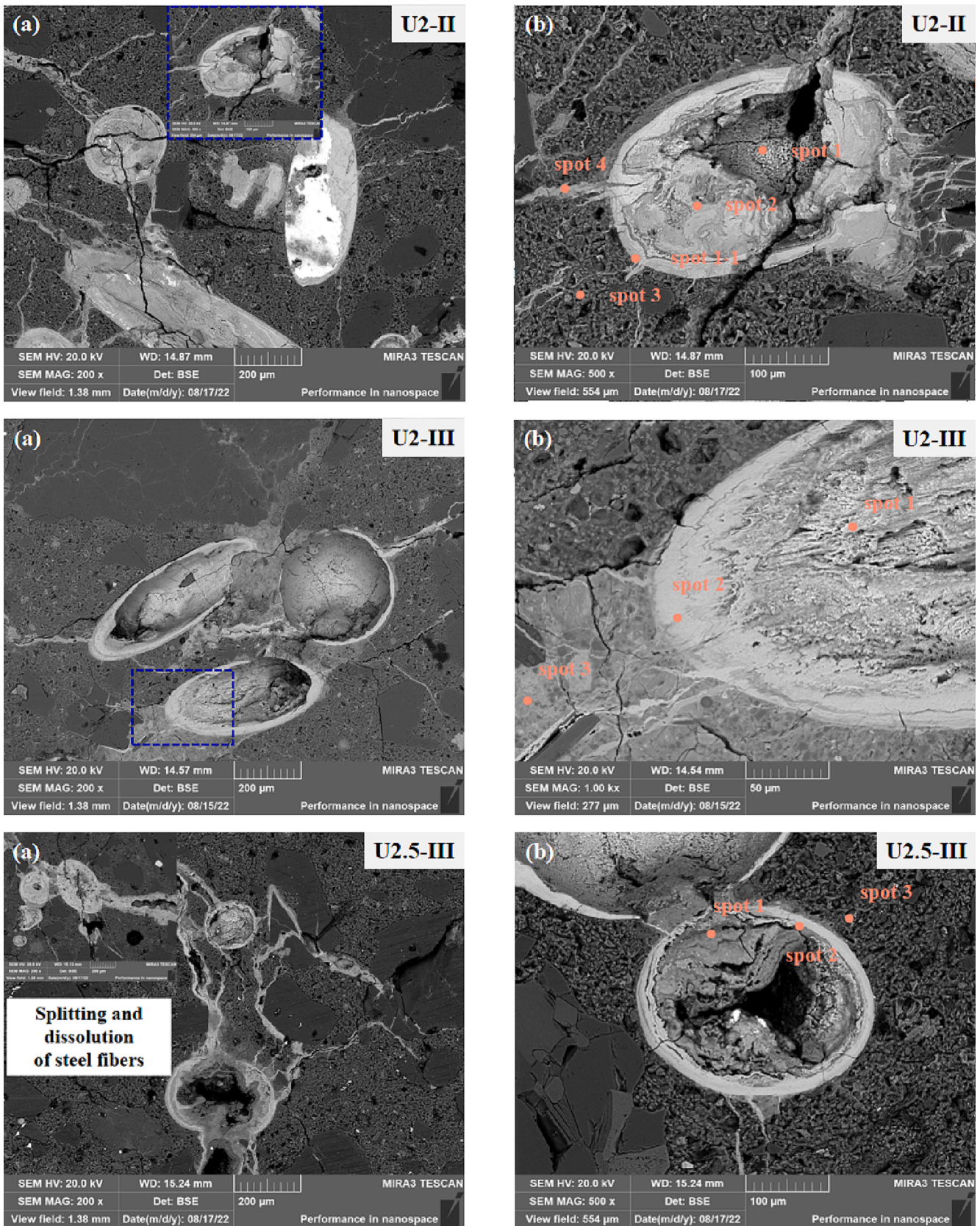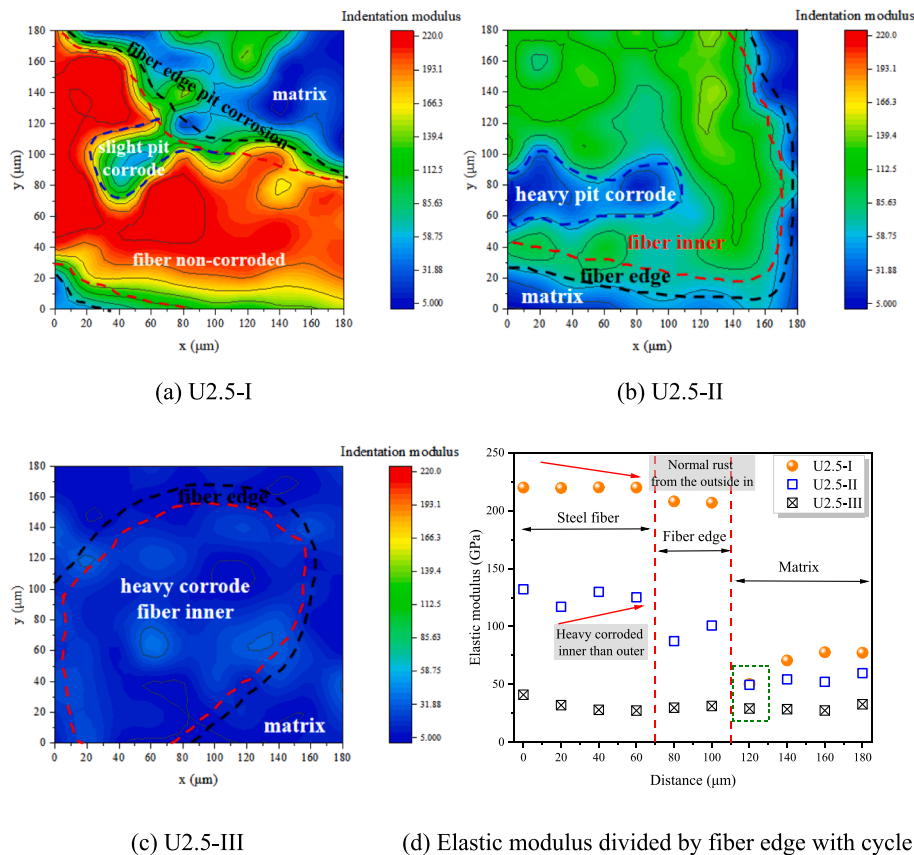
Fig. 7. (a) Representative SEM images, (b) EDS spot in the design samples.

Table 4

Analyzed Cl concentration, Fe/O atomic ratio in Figs. 7 and S1.

Sample	Spot	Position	Cl (wt%)	Fe/O atomic ration	Sample	Spot	Position	Cl (wt%)	Fe/O atomic ration
U2.5-I	1	non-corroded	/	/	U2.5-I	2	matrix	/	2.80
	1–1	fiber edge	/	2.35		3	matrix	/	0.02
U1-II	1	corroded	0.28	0.63	U1-III	1	corroded	/	0.58
	2	non-corroded	0.21	2.15		2	fiber edge	0.35	0.49
	3	fiber edge	0.31	0.87		3	matrix	0.51	0.03
	4	matrix	0.61	0.20	U1.5-III	1	corroded	/	0.50
U1.5-II	1	corroded	/	0.58		2	fiber edge	/	0.65
	2	fiber edge	0.57	0.40		3	matrix	/	0.25
	3	matrix	0.20	0.03	U2-III	1	corroded	0.29	1.32
U2-II	1	corroded	/	3.01					
	2	corroded	0.58	0.54		2	fiber edge	0.17	0.31
	1–1	fiber edge	0.87	0.36		3	matrix	0.61	0.34
	3	matrix	0.94	0.01	U2.5-III	1	non-corroded	0.21	1.41
	4	crack	0.62	0.31		2	corroded	0.13	0.70
U2.5-II	1	corroded	0.56	0.52		1–1	fiber edge	0.34	0.50
	2	fiber edge	0.55	0.28		3	matrix	0.39	0.06
	3	matrix	1.82	0.34					
U3-II	1	fiber	/	6.90	U3-III	1	fiber	1.26	0.71
	2	corroded	0.38	0.10		2	fiber edge	1.48	0.32
	1–1	fiber edge	0.42	1.04		3	corroded	1.63	0.07
	3	matrix	0.24	0.01		4	matrix	0.49	0.06

(a) U2.5-I   (b) U2.5-II

(c) U2.5-III   (d) Elastic modulus divided by fiber edge with cycle

Fig. 8. Nano-mechanical properties of UHPFRC with Corrosion I, II and III, (a ~ c) Contour map of indentation modulus of U2.5-I/II/III; (d) Elastic modulus distributions of the designed UHPFRC.

elastic modulus than matrix. However, when steel fiber was severely corroded and reached corrosion degree III, the elastic modulus of steel fiber decreased below 50 GPa. It can be found that the elastic modulus of matrix at the distance of 100 ~ 120 μm dropped clearly, then it gradually increased further away from fiber edge in matrix, as shown in Fig. 8 (d) and S3 (g). This is because pores are introduced around steel fiber [45]. Meanwhile, corrosion products further degrade the matrix near steel fibers.

3.4. Electrochemical properties of UHPFRC with various corrosion

In this work, corrosion time and fiber content are the two key factors to determine chloride resistance of UHPFRC. Polarization curves can offer relevant information about corrosion potential and current density to quantitatively evaluate the corrosion sensitivity of UHPFRC subjected corrosion. Fig. 9 (a) showed that potential decreased with an increasing corrosion degree from I to III under the same fiber amount, and
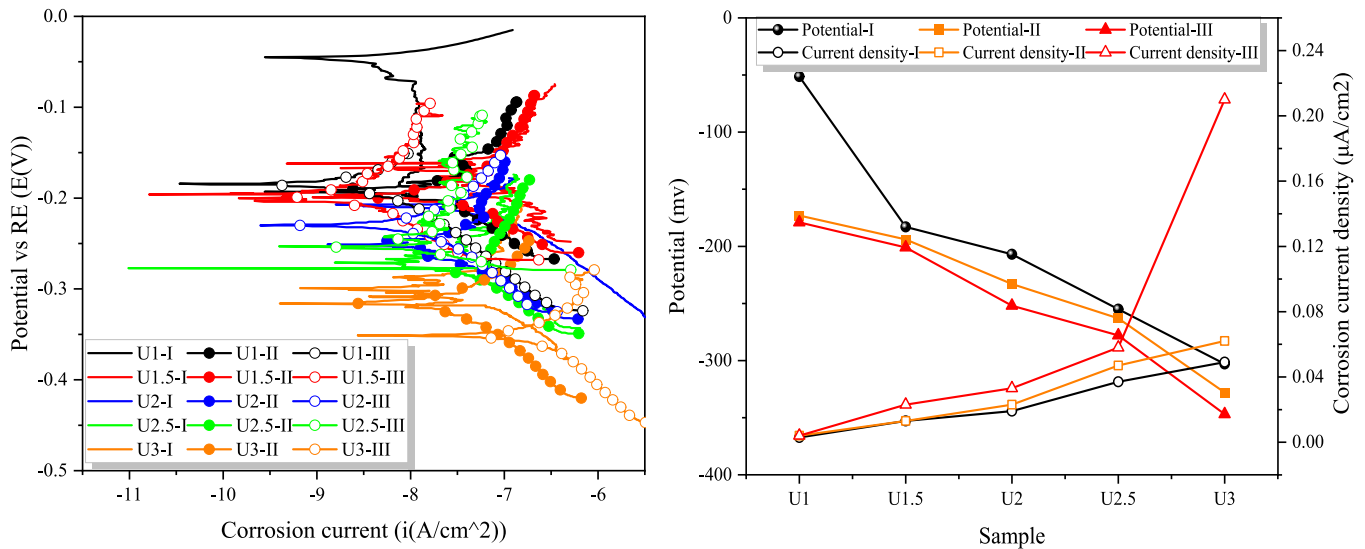
Fig. 9. (a) The measure curves of Tafel polarization; (b) fitted results of Tafel.

corrosion current density got a developing tendency, indicating severe corrosion occurred which is caused by continuous invasion of chloride. Meanwhile, the resistance in UHPFRC reduced with the increasing fiber contents under the same corrosion degree. The tendency of potential reduction in UHPFRC showed the following sequence under corrosion III: U3 < U2.5 < U2 < U1.5 < U1, same as that of corrosion I and II, shown in Fig. 9 (b). The trend of current density was opposite to that of corrosion potential, under the same corrosion degree. This further proves that the electrochemical corrosion increases with the increase of steel fiber content due to fiber network structure, consequently accelerating the corrosion development of UHPFRC [20,53]. Fiber corrosion rate is determined by fiber amounts and the contact between corrosive solution and fibers. The best-fit outcome for corrosion current density and potential, as shown in Fig. 9 (b), manifests that corrosion potential moves toward negative values with the increase of fiber contents and corrosion degree. As corrosion potential went down, corrosion current density increased gradually from 0.004 $\mu A/cm^2$ to 0.21 $\mu A/cm^2$ from 1 vol% to 3 vol% under corrosion III. In addition, corrosion current density was strengthened by the increase of corrosion degree under the same fiber amounts, as presented in Fig. 9 (b). All of these make clear the

occurrence of serious corrosion due to the development of corrosion time and increase of fiber amounts.

3.5. Mechanical performance degradation of UHPFRC with various corrosion degree

In this work, flexural-deflection and compressive strengths of UHPFRC were used to investigate the effects of fiber corrosion on the hardened behaviors, as shown in Fig. 10. Considering the special points of first cracking /ultimate flexural strength, all curves in Fig. 10 (a) can be divided into three stages, i.e. elastic ascending stage, nonlinear ascending stage (called strain hardening stage) and slow descending stage (called strain softening stage) with obvious saw teeth, which are consistent with previous researches [4,9,54,55]. These saw-teethes indicate that the improved strengthening effect is directly associated with fiber content. It can be observed that all ultimate flexural/first crack strength (Fig. 10 (a), detailed in Fig. S4) and compressive strength (Fig. 10 (b)), were increased with steel fiber content. Average values of compressive, ultimate flexural and first crack strength of U1-I were 126.2, 12.28 and 10.51 MPa, respectively. With fibers reaching to 3 vol
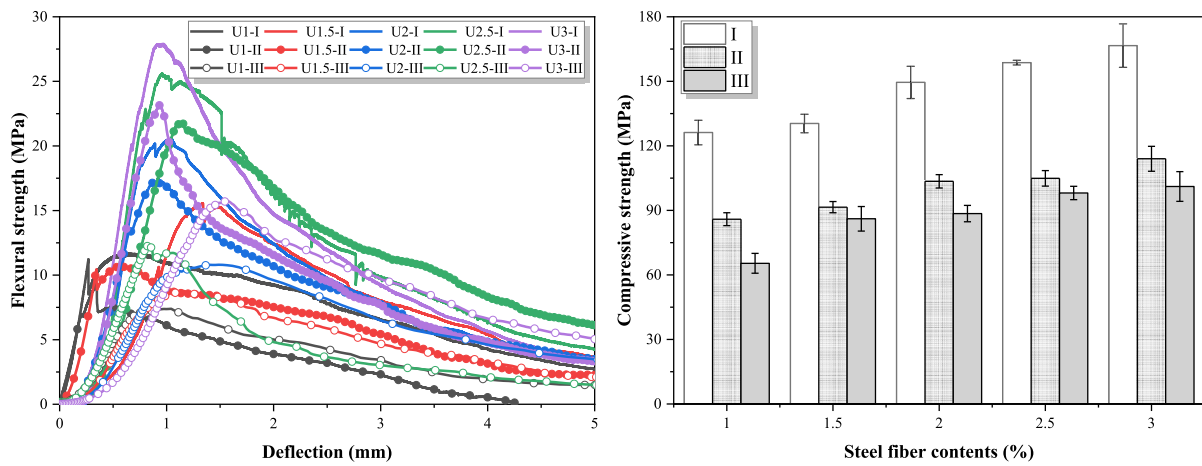
(a) Three-point flexural strength-deflection curve   (b) Compressive strength

Fig. 10. Effects of fiber corrosion on the compressive and flexural strength of UHPFRC.

%, the compressive, ultimate flexural and first crack strength (U3-I) as high as 166.6, 27.97 and 15.1 MPa were achieved. This can be attributed to that more fibers can effectively delay the crack growth and stabilize crack propagation [54,56]. More fibers can effectively overlap and decrease the average space between fibers, resulting in the improvement of strength by fibers to absorb a part of the matrix stress and sustain more load stress.

Clearly, all strength including ultimate flexural/first crack strength and compressive strength were reduced gradually with the increased corrosion degree under the same fiber amounts. The oxidation of steel fiber is promoted by the action of current and electrolyte solution in pore, and multi-fiber is more easy to generate galvanic corrosion, which accelerates the formation of rust (e.g. $Fe_2O_3 \cdot nH_2O$) on the surface of fiber [34]. With the increase of electrochemical acceleration time, the progressive oxidation of iron continues to produce rust, which decreases the effective volume of steel fiber. As volume of steel fiber decreases, its bridging performance and energy absorption capacity decrease, further, the presence of rust will produce a weak interface between concrete matrix and fiber. Finally, strength of UHPFRC greatly decreases with the increase of degree of rust. Fibers present different corrosion degree, and some fibers still remain partially bridging performance, resulting in resistance to matrix cracking. For instance, flexural/first crack strength and compressive strength of U2 were decreased from 20.62 to 10.8 MPa, 12.36 to 7.67 MPa, 149.5 to 88.5 MPa, respectively, with the increase of corrosion degree from no corrosion I to heavy corrosion III. The remaining data showed a similar tendency to U2, and results of other samples were presented in Fig. S4 and Table S1. This further confirms that the increase of corrosion time accelerates fiber corrosion, inducing fiber splitting and concrete cracking, even spalling of concrete cover (proven in Figs. 5 and 7), consequently resulting in the strength reduction of UHPFRC.

4. Discussions

During process of electrochemical corrosion, the corrosion evolution is complex [57,58]. Most studies focus on the corrosion of single reinforcement, but very few on multi-fiber corrosion, especially on the degradation of macroscopic mechanical properties of steel fiber corrosion in UHPFRC from the perspective of micromechanics. Corrosion evolution paths for UHPFRC with different fiber contents and corrosion degree on corrosion can be predicted according to morphology of corroded samples in this work. It can be well applied to investigate the corrosion induced degradation on UHPFRC through micro-/macro-mechanics.

4.1. Corrosion initiated at fiber edge

Characteristics of chloride ion and internal defects such that pores and interface between steel and concrete play a vital role in corrosion initiation [14,19,59,60]. According to above results, due to the poor connecting relationship among fibers at low contents (such that less than 2 vol%), steel fiber corrosion is mainly achieved by erosive solution through matrix defects (as an open corrosive channel) regardless of corrosion degrees. A conceptual model of the corrosion deterioration evolution in UHPFRC with poorly connected fibers at low contents is proposed in Fig. 11. This schematic diagram presents that the evolution of fiber corrosion in UHPFRC can be divided into three stages. First stage is continuous invasion of harmful substances under the action of electro-migration and independent diffusion. Weak interfacial zone between fibers and surrounding matrix is increased with the increase of fiber contents [45], which is convenient for the invasion of harmful ions, resulting in the increase of chloride concentration (see Fig. 6). Second stage is the continuous dissolution of iron. When chloride ions reaches a critical concentration [14,61], passive film degradation occurs. Then steel fibers turn to ionized state and dissolve subsequently, resulting in a reduction of corrosion potential in UHPFRC which further accelerates the corrosion initiation, as demonstrated in Fig. 9. Last stage is the generation and expansion of corrosion products. With the aggravation of fiber corrosion, the Fe/O atomic ratio of most locations in fiber edge is lower than that of fiber inner (shown in Table 4), which indicates corrosion is initiated at fiber edge with the constant invasion of oxygen, resulting in the degradation in elastic modulus and hardness of fiber edge than fiber inner (demonstrated in Figs. 8 and S3). Once the amount of corrosion product reaches a threshold, volume expansion is started [19], and the corrosion products preferentially fill the matrix around fiber edge, and then gradually permeate into matrix away from fiber. The expanding force induced by corrosion products would generate cracks, resulting in further acceleration of corrosion. The mechanical properties of UHPFRC are further degraded.

4.2. Heavy corrosion triggered from fiber center

Surprisingly, various cracks and pores occur in fiber center, as shown in SEM images of U2-II and U2.5-III (Figs. 7 and S1). Steel fibers with more than 2 vol% generate a well-connected conductive network, and large interfacial zones between fibers and nearby matrix which provide ample room for corrosive solution. Once the erosive solution arrives at fiber edge, it will accelerate fiber center corrosion through the gap impurities of fiber under the action of spontaneous current and macro-cell reaction caused by a well-connected fiber network. A schematic diagram
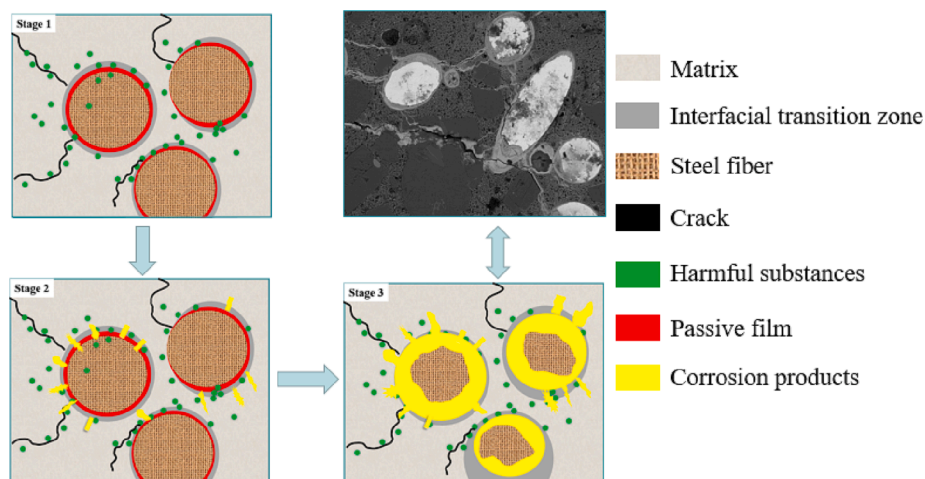

Fig. 11. Conceptual deterioration evolution model of corrosion mechanism in UHPFRC.

Matrix Interfacial transition zone Harmful substances Corroded fiber
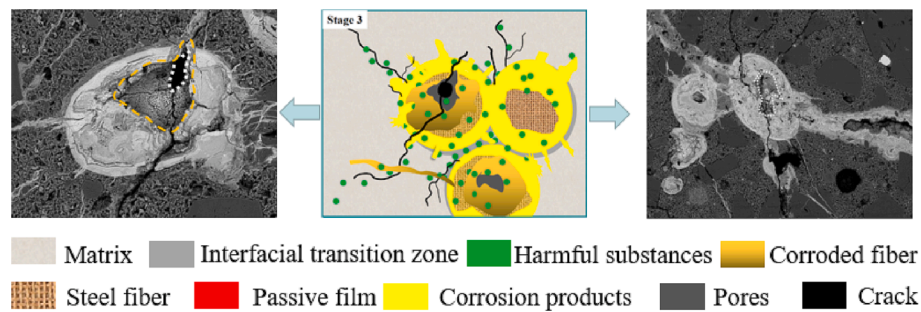Steel fiber Passive film Corrosion products Pores Crack

Fig. 12. Schematic illustration of the heavy rust in fiber center than outer in UHPFRC.

of heavy corrosion in fiber center than outer in UHPFRC is illustrated in Fig. 12, which mainly occurs at high fiber contents ($\geq$2 vol%) with a well-connected conductive network. After passive film is destroyed and fibers begin to corrode, harmful substances have penetrated into fiber center along the impurity-induced weak interfaces in fibers caused by manufacture. Water, oxygen and corrosive ions would arrive at fiber center surface directly through cracks. Then corrosive solution accumulates in fiber center, leading to a high concentration of chloride ions inside. Meanwhile, heavily corroded fiber, slightly corroded fiber and crack/uncrack position would show a potential difference, which is similar to the two steel corroded in one specimen generating macro-cell corrosion [62]. Due to the electric field of well-connected fiber network in concrete, macro-cell corrosion occurs. It contributes to degradation not only in fiber network zone by different damage degree of fiber center and corrosion products, but also in the global region of steel fibers and matrix through multi-ion actions. Therefore, corrosion products are generated and developed from inner to outer with the volume expansion force, destroying the structural integrity of steel fibers. In case of U2-III, a higher chloride ion concentration reaches 0.29 wt% at fiber inner than fiber edge of 0.17 wt%, resulting in a heavy corrosion appearance in fiber inner other than outer (see in Fig. 7 and Table 4).

The data shown in Section 3 of this work reveal the effects of fiber corrosion degree on the mechanical performance degradation of UHPFRC at a multiscale, the results above indicated that the fiber corrosion significantly reduced the mechanical performance of cement-based composites, as well as weakened the bonding interface between steel fiber and matrix [29]. In general, chloride-induced corrosion and cracking from outer environment to the inner matrix and steel fibers are a complex process, where the invasion of harmful ions including physical absorption and chemical binding, and the electrochemical reaction generated by the potential difference between the matrix pore solution and fibers through the pore or micro-crack, would make a detrimental impact. In agreement with previous research [53], chloride ions first destroy the passivation layer of the steel fiber, then the corrosion of iron will occur following the reaction in case of aerobic and anaerobic conditions: $Fe + 0.75\,O_2 + 0.5\,H_2O = FeOOH$ and $3\,Fe + 4\,H_2O = Fe_3O_4 + 4\,H_2$.

When steel fibers subjected a light corrosion damage or without corrosion, the macro-mechanical properties of UHPFRC can be developed with increasing fiber amounts (see in Fig. 10), which is attributed to that fibers can still significantly play bridging role, effectively alleviating matrix stress. U3-I achieves the highest increase of 1.28 times in flexural strength, 44% in first crack strength and 32% in compressive strength, respectively, compared with that of U1-I. When corrosion degree deepens that leads to a serious pit corrosion or even fiber fracture, matrix plays a dominant role, and the deterioration is inevitable. As stated in Section 3, all mechanical properties are gradually declined by the increase of corrosion degree under the same fiber amounts, presented in Figs. 10 and S4 (data detailed in Table S1). Under the action of chemical and current potential difference, Cl⁻, O_2 and H_2O move with the solution from micro-crack of matrix to fiber edge or accumulate in fiber inner through weak interface, leading to the expansion of micro-

cracks in fiber or matrix under the force of corrosion products. It is important to note that corrosion area will move further to surrounding matrix as fibers dissolve and are subsequently badly corroded, causing the reaction or degradation of corrosion products and matrix. As stated in Figs. 8 and S3, contact regions between corroded fibers and matrix are weak, resulting in a lower elastic modulus and nano-hardness at the matrix near fiber edge than that matrix far away from fiber edge. That is to say that the combination of the two (fiber corrosion and rust expanding into matrix) greatly decreases mechanical properties of UHPFRC.

5. Conclusions

This study investigates the deterioration of UHPFRC with five fiber contents subjected three corrosion degree of I (no corrosion), II (slight corrosion) and III (heavy corrosion) from macro-/micro- perspective. Two conceptual corrosion models of steel fibers are proposed to describe the deterioration evolution of UHPFRC. The main conclusions can be drawn as follows:

1. A longer corrosive immersion duration and greater fiber amounts generate a severer strength reduction in UHPFRC, resulting from the dissolution and cracking in fiber and damage in concrete matrix. In particular, a sever flexural strength reduction of up to 47% in UHPFRC was found at a high corrosion degree.
2. Corrosion time and fiber contents impact the electrochemical resistance in UHPFRC. With the fiber volume fraction increases from 1 vol% to 3 vol% under corrosion III, current density increasing from 0.004 μA/cm^2 to 0.21 μA/cm^2 indicates fiber corrosion increased.
3. Deterioration of matrix starts with the accumulation of aggressive solution, followed by fiber dissolution. Chloride depth and iron concentration in UHPFRC are both enhanced with the increase of fiber content and corrosion degree. The values of iron ion at the surface are steadily increased from 327.1 to 343.9 mg/L with fiber contents from 1 vol% to 2.5 vol%, with the highest up to 597.2 mg/L at 3 vol% under corrosion III. This is attributed to that the increased defects and iron brought by increased fiber contents accelerates iron dissolution continuously in the matrix.
4. The essence of macroscopic mechanical performance reduction is the degradation of microstructure and microscopic mechanics caused by fiber corrosion. A decreasing tendency of Fe/O atomic ratio is associated directly with the invasion of O_2, resulting in that elastic modulus and nano-hardness of fiber and matrix decrease with the increase of fiber contents and corrosion degree. Due to the formation and expansion of fiber corrosion products, matrix near the fiber edge 20 μm is preferentially affected, whose elastic modulus drops at least 10% more than matrix far away fiber edge.
5. The influence of fiber on the corrosion morphology selection differs significantly at low and high fiber contents. The conventional fiber corrosion path of matrix-fiber edge-fiber inner, mainly occurs at a lower fiber content of less than 2 vol At high fiber contents ($\geq$2 vol %), another corrosion path originates from fiber inner outward to

matrix, due to the gap impurities and macro cell corrosion caused by a well-connected conductive network. The erosive medium gathers in fiber center and trigger corrosion, resulting in the cracking of steel fibers, then destroying the fiber structural integrity. Corrosion products continuously squeeze the surrounding matrix, leading to the increase of cracks and reduction on the strength.

CRediT authorship contribution statement

Zhaoping Song: Writing – original draft, Methodology, Investigation, Formal analysis, Data curation. **Shaohua Li:** Writing – review & editing, Supervision, Investigation. **Qingliang Yu:** Writing – review & editing, Supervision, Project administration, Methodology, Funding acquisition, Conceptualization.

Declaration of Competing Interest

The authors declare that they have no known competing financial interests or personal relationships that could have appeared to influence the work reported in this paper.

Data availability

Data will be made available on request.

Acknowledgment

Appendix A. Supplementary data

Supplementary data to this article can be found online at https://doi.org/10.1016/j.conbuildmat.2023.132329.

References

[1] Q. Yu, W. Zhuang, C. Shi, Research progress on the dynamic compressive properties of ultra-high performance concrete under high strain rates, Cem. Concr. Compos. 124 (2021), 104258, https://doi.org/10.1016/j.cemconcomp.2021.104258.

[2] P.P. Li, H.J.H. Brouwers, Q. Yu, Influence of key design parameters of ultra-high performance fibre reinforced concrete on in-service bullet resistance, Int. J. Impact Eng. 136 (2020), 103434.

[3] P. Zhang, Y.N. Zhao, Q.F. Li, P. Wang, T.H. Zhang, Flexural toughness of steel fiber reinforced high performance concrete containing nano-SiO2 and fly ash, Sci. World J. 2014 (2014), https://doi.org/10.1155/2014/403743.

[4] Q. Zheng, C. Li, B. He, Z. Jiang, Revealing the effect of silica fume on the flexural behavior of ultra-high-performance fiber-reinforced concrete by acoustic emission technique, Cem. Concr. Compos. 131 (2022), 104563, https://doi.org/10.1016/j.cemconcomp.2022.104563.

[5] M. Gesoglu, E. Güneyisi, G.F. Muhyaddin, D.S. Asaad, Strain hardening ultra-high performance fiber reinforced cementitious composites: Effect of fiber type and concentration, Compos. Part B Eng. 103 (2016) 74–83, https://doi.org/10.1016/j.compositesb.2016.08.004.

[6] P.P. Li, M.J.C. Sluijsmans, H.J.H. Brouwers, Q.L. Yu, Functionally graded ultra-high performance cementitious composite with enhanced impact properties, Compos. Part B Eng. 183 (2020), 107680.

[7] N.M. Azmee, N. Shafiq, Ultra-high performance concrete: From fundamental to applications, Case Stud. Constr. Mater. 9 (2018), e00197.

[8] Y.Y.Y. Cao, Q.L. Yu, P.P. Li, H.J.H. Brouwers, Q.L. Yu-Assistant, H.J.H. Brouwers-Professor, Effects of Fiber Content on Mechanical Properties of UHPFRC with Coarse Aggregates, (n.d.) 3–10.

[9] S. Li, O.M. Jensen, Q. Yu, Mechanism of rate dependent behaviour of ultra-high performance fibre reinforced concrete containing coarse aggregates under flexural loading, Constr. Build. Mater. 301 (2021), 124055, https://doi.org/10.1016/j.conbuildmat.2021.124055.

[10] T.E.T. Buttignol, J.L.A.O. Sousa, T.N. Bittencourt, Ultra High-Performance Fiber-Reinforced Concrete (UHPFRC): a review of material properties and design procedures, Rev. IBRACON Estruturas e Mater. 10 (2017) 957–971, https://doi.org/10.1590/s1983-41952017000400011.

[11] Q. Song, R. Yu, Z. Shui, S. Rao, X. Wang, M. Sun, C. Jiang, Steel fibre content and interconnection induced electrochemical corrosion of Ultra-High Performance Fibre Reinforced Concrete (UHPFRC), Cem. Concr. Compos. 94 (2018) 191–200, https://doi.org/10.1016/j.cemconcomp.2018.09.010.

[12] D.-Y. Yoo, W. Shin, B. Chun, N. Banthia, Assessment of steel fiber corrosion in self-healed ultra-high-performance fiber-reinforced concrete and its effect on tensile performance, Cem. Concr. Res. 133 (2020), 106091.

[13] D.Y. Yoo, K.H. Min, J.H. Lee, Y.S. Yoon, Shrinkage and cracking of restrained ultra-high-performance fiber-reinforced concrete slabs at early age, Constr. Build. Mater. 73 (2014) 357–365, https://doi.org/10.1016/j.conbuildmat.2014.09.097.

[14] V. Marcos-Meson, A. Michel, A. Solgaard, G. Fischer, C. Edvardsen, T.L. Skovhus, Corrosion resistance of steel fibre reinforced concrete - A literature review, Cem. Concr. Res. 103 (2018) 1–20, https://doi.org/10.1016/j.cemconres.2017.05.016.

[15] L. Hou, Y. Peng, R. Xu, X. Zhang, T. Huang, D. Chen, Corrosion behavior and flexural performance of reinforced SFRC beams under sustained loading and chloride attack, Eng. Struct. 242 (2021) 112553, https://doi.org/10.1016/j.engstruct.2021.112553.

[16] J.P. Kaufmann, Durability performance of fiber reinforced shotcrete in aggressive environment, WTC 2014 – Tunnels a Better Life 303 (2014) 1–7.

[17] S. Wang, X. Guo, Z. Guo, C. He, X. Duan, W. Hu, K. Zhuang, Direct characterization of steel fibre corrosion in pre-cracked ultra-high performance concrete (UHPC) with different crack widths, Constr. Build. Mater. 315 (2022), 125769, https://doi.org/10.1016/j.conbuildmat.2021.125769.

[18] W. Shin, D.Y. Yoo, Influence of steel fibers corroded through multiple microcracks on the tensile behavior of ultra-high-performance concrete, Constr. Build. Mater. 259 (2020), 120428, https://doi.org/10.1016/j.conbuildmat.2020.120428.

[19] W. Xu, Y.u. Li, H. Li, K. Wang, C. Zhang, Y. Jiang, S. Qiang, Corrosion mechanism and damage characteristic of steel fiber concrete under the effect of stray current and salt solution, Constr. Build. Mater. 314 (2022), 125618.

[20] L.S. Lv, J.Y. Wang, R.C. Xiao, M.S. Fang, Y. Tan, Influence of steel fiber corrosion on tensile properties and cracking mechanism of ultra-high performance concrete in an electrochemical corrosion environment, Constr. Build. Mater. 278 (2021), 122338, https://doi.org/10.1016/j.conbuildmat.2021.122338.

[21] K. Hashimoto, T. Toyoda, H. Yokota, K. Kono, T. Kawaguchi, Tension-softening behavior and chloride ion diffusivity of cracked ultra high strength fiber reinforced concrete, RILEM-Fib-AFGC Int. Symp. Ultra-High Perform. Fibre-Reinforced Concr. UHPFRC 2013. (2013) 257–264.

[22] A.M. Matos, S. Chaves Figueiredo, S. Nunes, E. Schlangen, J.L. Barroso-Aguiar, Durability of an UHPFRC under mechanical and chloride loads, Constr. Build. Mater. 311 (2021), 125223.

[23] S. Pyo, T. Koh, M. Tafesse, H.K. Kim, Chloride-induced corrosion of steel fiber near the surface of ultra-high performance concrete and its effect on flexural behavior with various thickness, Constr. Build. Mater. 224 (2019) 206–213, https://doi.org/10.1016/j.conbuildmat.2019.07.063.

[24] L. Fan, W. Meng, L. Teng, K.H. Khayat, Effect of steel fibers with galvanized coatings on corrosion of steel bars embedded in UHPC, Compos. Part B Eng. 177 (2019), 107445, https://doi.org/10.1016/j.compositesb.2019.107445.

[25] G. Shu, Q. Zhang, Y. Huang, Y. Bu, Micromechanical Analysis of Steel Fiber Corrosion in Ultra-high Performance Concrete, Xinan Jiaotong Daxue Xuebao/Journal Southwest Jiaotong Univ Chinese 54 (2019) 1268–1276, https://doi.org/10.3969/j.issn.0258-2724.20170453.

[26] L. Hou, Z. Ye, B. Zhou, C. Shen, F. Aslani, D. Chen, Bond behavior of reinforcement embedded in steel fiber reinforced concrete under chloride attack, Struct. Concr. 20 (2019) 2242–2255, https://doi.org/10.1002/suco.201800246.

[27] J.L. Granju, S.U. Balouch, Corrosion of steel fibre reinforced concrete from the cracks, Cem. Concr. Res. 35 (2005) 572–577, https://doi.org/10.1016/j.cemconres.2004.06.032.

[28] D.Y. Yoo, W. Shin, Improvement of fiber corrosion resistance of ultra-high-performance concrete by means of crack width control and repair, Cem. Concr. Compos. 121 (2021), 104073, https://doi.org/10.1016/j.cemconcomp.2021.104073.

[29] V. Marcos-Meson, M. Geiker, G. Fischer, A. Solgaard, U.H. Jakobsen, T. Danner, C. Edvardsen, T.L. Skovhus, A. Michel, Durability of cracked SFRC exposed to wet-dry cycles of chlorides and carbon dioxide – Multiscale deterioration phenomena, Cem. Concr. Res. 135 (2020), 106120, https://doi.org/10.1016/j.cemconres.2020.106120.

[30] S. Pyo, M. Tafesse, H. Kim, H.K. Kim, Effect of chloride content on mechanical properties of ultra high performance concrete, Cem. Concr. Compos. 84 (2017) 175–187, https://doi.org/10.1016/j.cemconcomp.2017.09.006.

[31] A. Beglarigale, H. Yazıcı, Electrochemical corrosion monitoring of steel fiber embedded in cement based composites, Cem. Concr. Compos. 83 (2017) 427–446, https://doi.org/10.1016/j.cemconcomp.2017.08.004.

[32] L. Fan, W. Meng, L. Teng, K.H. Khayat, Effects of lightweight sand and steel fiber contents on the corrosion performance of steel rebar embedded in UHPC, Constr. Build. Mater. 238 (2020), 117709, https://doi.org/10.1016/j.conbuildmat.2019.117709.

[33] N. El-Joukhadar, S.J. Pantazopoulou, Effectiveness of UHPFRC cover in delaying bar corrosion, Constr. Build. Mater. 269 (2021), 121288, https://doi.org/10.1016/j.conbuildmat.2020.121288.

[34] D.Y. Yoo, W. Shin, B. Chun, Corrosion effect on tensile behavior of ultra-high-performance concrete reinforced with straight steel fibers, Cem. Concr. Compos. 109 (2020), 103566, https://doi.org/10.1016/j.cemconcomp.2020.103566.

[35] M. Miller, C. Bobko, M. Vandamme, F.J. Ulm, Surface roughness criteria for cement paste nanoindentation, Cem. Concr. Res. 38 (2008) 467–476, https://doi.org/10.1016/j.cemconres.2007.11.014.

[36] G.M.P.W.C. Oliver, An improved technique for determining hardness and elastic modulus using load and displacement sensing indentation experiments, J. Mater. Res. 7 (1992) 1564–1583, https://doi.org/10.1177/003591571901200704.

[37] C. Paste, Nano-indentation Character of Interfacial Transition Zone Between Steel Fiber and Cement Paste, J. CHINESE Ceram. Soc. (2016).

[38] C. Wen, Y. Tian, Z. Mai, J. Hu, G. Wang, Effect of macropores at the steel-concrete interface on localized corrosion behaviour of steel reinforcement, Cem. Concr. Compos. 129 (2022), 104510, https://doi.org/10.1016/j.cemconcomp.2022.104510.

[39] A. Hajiesmaeili, E. Denarié, Capillary flow in UHPFRC with synthetic fibers, under high tensile stresses, Cem. Concr. Res. 143 (2021), 106368.

[40] S. Shagñay, A. Bautista, J. Donaire, M. Torres-Carrasco, D.M. Bastidas, F. Velasco, Chloride-induced corrosion of steel reinforcement in mortars manufactured with alternative environmentally-friendly binders, Cem. Concr. Compos. 130 (2022), 104557, https://doi.org/10.1016/j.cemconcomp.2022.104557.

[41] F. Tang, G. Chen, J.S. Volz, R.K. Brow, M.L. Koenigstein, Cement-modified enamel coating for enhanced corrosion resistance of steel reinforcing bars, Cem. Concr. Compos. 35 (2013) 171–180, https://doi.org/10.1016/j.cemconcomp.2012.08.009.

[42] A. Pourjahanshahi, H. Madani, Chloride diffusivity and mechanical performance of UHPC with hybrid fibers under heat treatment regime, Mater. Today Commun. 26 (2021), 102146, https://doi.org/10.1016/j.mtcomm.2021.102146.

[43] A.S. El-dieb, Mechanical, durability and microstructural characteristics of ultra-high-strength self-compacting concrete incorporating steel fibers, Mater. Des. 30 (2009) 4286–4292, https://doi.org/10.1016/j.matdes.2009.04.024.

[44] W. Zhuang, S. Li, Z. Wang, Z. Zhang, Q. Yu, Impact of micromechanics on dynamic compressive behavior of ultra-high performance concrete containing limestone powder, Compos. Part B Eng. 243 (2022), 110160, https://doi.org/10.1016/j.compositesb.2022.110160.

[45] R. Yu, P. Spiesz, H.J.H. Brouwers, Mix design and properties assessment of Ultra-High Performance Fibre Reinforced Concrete (UHPFRC), Cem. Concr. Res. 56 (2014) 29–39, https://doi.org/10.1016/j.cemconres.2013.11.002.

[46] N. Banthia, C. Foy, Marine Curing of Steel Fiber Composites, J. Mater. Civ. Eng. 1 (2) (1989) 86–96.

[47] Z. Ai, W. Sun, J. Jiang, Recent status of research on corrosion of low alloy corrosion resistant steel and analysis on existing eroblems, Corros. Sci. Prot. Technol. 27 (2015) 525–536. https://doi.org/10.11903/1002.6495.2014.407.

[48] B. Jiang, K. Doi, K. Tsuchiya, Y. Kawano, A. Kori, K. Ikushima, Micromechanical properties of steel corrosion products in concrete studied by nano-indentation technique, Corros. Sci. 163 (2020), 108304, https://doi.org/10.1016/j.corsci.2019.108304.

[49] J. Monnier, D. Neff, S. Réguer, P. Dillmann, L. Bellot-Gurlet, E. Leroy, E. Foy, L. Legrand, I. Guillot, A corrosion study of the ferrous medieval reinforcement of the Amiens cathedral. Phase characterisation and localisation by various microprobes techniques, Corros. Sci. 52 (2010) 695–710, https://doi.org/10.1016/j.corsci.2009.10.028.

[50] P. Zhan, J. Xu, J. Wang, C. Jiang, Multi-scale study on synergistic effect of cement replacement by metakaolin and typical supplementary cementitious materials on

properties of ultra-high performance concrete, Constr. Build. Mater. 307 (2021), 125082, https://doi.org/10.1016/j.conbuildmat.2021.125082.

[51] Y. Rui, L. Kangning, Y. Tianyi, T. Liwen, D. Mengxi, S. Zhonghe, Comparative study on the effect of steel and polyoxymethylene fibers on the characteristics of Ultra-High Performance Concrete (UHPC), Cem. Concr. Compos. 127 (2022), 104418, https://doi.org/10.1016/j.cemconcomp.2022.104418.

[52] Y. Zhao, H. Dai, W. Jin, A study of the elastic moduli of corrosion products using nano-indentation techniques, Corros. Sci. 65 (2012) 163–168, https://doi.org/10.1016/j.corsci.2012.08.016.

[53] A. Mancini, B. Lothenbach, G. Geng, D. Grolimund, D.F. Sanchez, S.C. Fakra, R. Dähn, B. Wehrli, E. Wieland, Iron speciation in blast furnace slag cements, Cem. Concr. Res. 140 (2021), 106287.

[54] B. Mobasher, A. Li, Y. Yao, A. Arora, N. Neithalath, Characterization of toughening mechanisms in UHPC through image correlation and inverse analysis of flexural results, Cem. Concr. Compos. 122 (2021), 104157, https://doi.org/10.1016/j.cemconcomp.2021.104157.

[55] Z. Wu, C. Shi, W. He, Comparative study on flexural properties of ultra-high performance concrete with supplementary cementitious materials under different curing regimes, Constr. Build. Mater. 136 (2017) 307–313, https://doi.org/10.1016/j.conbuildmat.2017.01.052.

[56] Z. Wu, C. Shi, W. He, L. Wu, Effects of steel fiber content and shape on mechanical properties of ultra high performance concrete, Constr. Build. Mater. 103 (2016) 8–14, https://doi.org/10.1016/j.conbuildmat.2015.11.028.

[57] M. Pourbaix, Thermodynamics and corrosion, Corros. Sci. 30 (10) (1990) 963–988.

[58] J.Y. Hu, S.S. Zhang, E. Chen, W.G. Li, A review on corrosion detection and protection of existing reinforced concrete (RC) structures, Constr. Build. Mater. 325 (2022), 126718.

[59] H. Zheng, J. Lu, P. Shen, L. Sun, C.S. Poon, W. Li, Corrosion behavior of carbon steel in chloride-contaminated ultra-high-performance cement pastes, Cem. Concr. Compos. 128 (2022), 104443, https://doi.org/10.1016/j.cemconcomp.2022.104443.

[60] J. Shi, X. Guan, J. Ming, X. Zhou, Improved corrosion resistance of reinforcing steel in mortars containing red mud after long-term exposure to aggressive environments, Cem. Concr. Compos. 130 (2022), 104522, https://doi.org/10.1016/j.cemconcomp.2022.104522.

[61] J.P. Hwang, M.S. Jung, M. Kim, K.Y. Ann, Corrosion risk of steel fibre in concrete, Constr. Build. Mater. 101 (2015) 239–245, https://doi.org/10.1016/j.conbuildmat.2015.10.072.

[62] Z.H. Jin, C. Jiang, X.L. Gu, Z. Dong, Macro-cell corrosion between crossed steel bars in cracked concrete, Constr. Build. Mater. 350 (2022), 128867, https://doi.org/10.1016/j.conbuildmat.2022.128867.